GEOPHYSICAL RESEARCH LETTERS, VOL. 24, NO.8, PAGES 987-990, APRIL 15, 1997

High time resolution study of the hemispheric power carried by energetic electrons into the ionosphere during the May 19/20, 1996 auroral activity

D. Lummerzheim, [1] M. Brittnacher, [2] D. Evans, [3] G. A. Germany, [4]
G. K. Parks, [2] M. H. Rees, [1,5] and J. F. Spann [6]

Abstract. The ultraviolet imager (UVI) on board the POLAR satellite offers the opportunity to obtain high time resolution global auroral images. The spectral discrimination of the imager is sufficient to separate the auroral far ultraviolet emissions from the scattered sunlight, even when the entire auroral zone is sunlit. The energy flux of the precipitating electrons is derived from the surface brightness through the LBH-long filter. Global images which have the dayglow removed are spatially integrated to yield the total rate of energy input into the northern hemisphere. This parameter, the hemispheric power, has found much application in ionospheric modeling. It can also be derived from electron spectra measured along the track of the NOAA/TIROS satellites that are combined with average empirical auroral precipitation patterns. We show that the hemispheric power derived from the two-dimensional images represents a substantial improvement in the temporal variability of this parameter. We present an example for the period of 19/20 May 1996 by comparing the hemispheric power derived from NOAA/TIROS measurements with those derived from the UVI images.

1. Introduction

The integrated hemispheric energy flux carried by auroral electron precipitation into the ionosphere is a measurable parameter of the rate of energy dissipation associated with auroral activity. This parameter, the hemispheric power, has already been used for several years in global models of the thermosphere and ionosphere [*Roble et al.*, 1988; *Fuller-Rowell et al.*, 1994; *Lu et al.*, 1995] to account for the influence of auroral ionization and finds application as an index to scale statistical auroral precipitation patterns. It is based on energetic electron and ion precipitation measured during passes of the NOAA/TIROS satellites over the aurora [*Evans*, 1987; *Fuller-Rowell and Evans*, 1987]. At an altitude of about 800 km these satellites traverse the auroral oval in about 25 minutes, yielding measurements of the electron and ion energy flux along the orbital track at an approximate 100 minute repetition rate for each hemisphere. The hemispheric power is derived from these measurements by fitting statistical precipitation patterns to the observations, thus extrapolating to the entire auroral oval. Clearly, the hemispheric power estimate based on *in situ* particle measurements relies on selective and very small sampling rates, and the required extrapolation and averaging result in masking the actual variability of the energy flux into the ionosphere.

To remedy this deficiency it is essential to acquire measurements of the energy flux simultaneously over the entire polar region and at a time resolution commensurate with auroral variability. It has become possible to extract this information from global auroral images taken from the POLAR satellite. The ultraviolet imager (UVI) acquires auroral images of the N_2(LBH) (Lyman-Birge-Hopfield) brightness which is proportional to the electron energy flux. The spectral resolution of the imager is sufficient to isolate the LBH bands from nearby OI lines and to separate the auroral brightness from the scattered sunlight, thus allowing interpretation of the images in conditions where the auroral oval is in sunlight.

2. Interpretation of UVI auroral images

The UVI instrument is described in detail by *Torr et al.* [1995]. The two N_2(LBH) filters of the UVI instrument are designed such that one (LBH-short) has a passband around 150 nm, which is dominated by N_2(LBH, $\Delta v = 0$ and $\Delta v = 1$) and where absorption by the Schuman-Runge continuum is strong, while the other (LBH-long) is centered near 170 nm with a passband dominated by N_2(LBH, $\Delta v = 4$), where there is little absorption. The emission rate of the N_2(LBH) bands is proportional to the incident energy flux, while the mean energy of the precipitating auroral electrons determines the altitude of the emission [*Strickland et al.*, 1983; *Rees et al.*, 1995]. Monitoring the brightness of emission features that suffer atmospheric extinction simultaneously with auroral features that are unattenuated by the atmosphere yields both energy flux and characteristic energy of the precipitation. Only the former is discussed in this note.

In the sunlit atmosphere N_2(LBH) emissions are also excited by photoelectrons. In order to obtain the inci-

[1] Geophysical Institute, University of Alaska, Fairbanks
[2] University of Washington, Geophysics Program, Seattle
[3] NOAA, Space Environment Center, Boulder, Colorado
[4] University of Alabama, Huntsville
[5] University of Southampton, Southampton, UK
[6] Marshall Space Flight Center, Huntsville, Alabama

Paper number 96GL03828
0094-8534/97/96GL-03828$05.00

dent energy flux over the entire auroral zone, we must distinguish between the aurora and scattered sunlight, and dayglow brightness where the aurora is sunlit. *Immel et al.* [1996] subtract the solar component of the image brightness in Dynamics Explorer images by using fitted dayglow functions that account for solar activity and viewing geometry. For a given solar activity level, the solar component in the UV brightness for a nadir looking geometry is a function of the local solar zenith angle. Off nadir viewing requires additional corrections for the slant path. In the following analysis we limit ourselves to nadir looking images where we can neglect the off nadir corrections, and assume that the solar contribution to the brightness of the UVI images is only a function of the solar zenith angle. Rather than using fitted functions as applied by *Craven et al.* [1994] and *Immel et al.* [1996], we determine the solar contribution for each image individually.

The technique for removing the solar contribution works as follows. For a given image, we determine the geographic and geomagnetic location of the volume of atmosphere that constitutes the source of the emission for each image pixel, assuming an emission height of 120 km. We then determine the local solar zenith angle for each of these volumes and sort them into bins of common solar zenith angles. Taking the average of the pixels in each bin, excluding pixels which fall into the auroral zone, gives the solar contribution to the pixels in the bin under consideration. Subtracting that value from all pixels with the same solar zenith angle, we are left with the auroral brightness. This is demonstrated in figure 1 with an image taken at 20:30 UT on May 19, 1996. The upper left panel shows the original UVI image, using the LBH-long filter. The imager subtends only a portion of the hemisphere, but includes the entire auroral oval. The Sun illuminated the Earth from the upper right direction. The entire aurora is in bright sunlight, and the terminator is in the lower left hand corner. Superimposed on the image is a strip of pixels with solar zenith angle between 70° and 72°. The line graph below shows the count rates of all pixels in this strip as a function of position along the strip. Also shown is the level of the solar contribution, computed as the average of the count rate of the pixels outside the interval between 62° and 77° geomagnetic latitude, indicated by the black part of the strip. This process is repeated for all 2° bins of solar zenith angle, leaving only the auroral brightness as shown in the upper right panel of figure 1. An animation demonstrating this process is available on the web at URL: `http://loke.gi.alaska.edu`.

Using an auroral model [*Lummerzheim and Lilensten*, 1994] we calculate the expected brightness of various UV emissions from a specified incident electron flux. Convolving this synthetic auroral spectrum with the instrument response gives the count rate for a given energy flux. The count rate using the LBH-long filter is almost independent of the mean energy of the auroral electrons, (and therefore altitude of the emission), and can be scaled to obtain the incident energy flux carried by energetic electrons. This interpretation of the images assumes that the contribution to the brightness from proton precipitation is negligible. The image is then transformed onto an apex geomagnetic coordinate grid. Integrating the flux over the transformed image yields the hemispheric power.

Uncertainties in the energy flux and hemispheric power stem from the calibration of the instrument and from the assumptions that went into the modeling. Cross sections for electron scattering, and cross sections for photon emission and absorption may contribute as much uncertainty as the calibration (about 20%). These errors apply equally to all pixels and at all times, while the error introduced by the airglow removal and neglecting the slant path of the viewing geometry has a systematic variation across an image. For an 8° field of view and nadir viewing from an altitude of 8 R_E at apogee, the slant path at the edge of the image is about 11% longer than the modeled vertical path. The method used to remove the airglow from the images does not distinguish between airglow and emissions due to polar rain inside the polar cap and would overestimate the airglow in the presence of polar precipitation. Close examination of figure 1 may suggest that the brightness inside the polar cap (pixel position 700 to 1200) is higher than equatorward of the aurora (pixel position 0 to 300). However, this difference is too small to be significant in the framework of this study.

3. Hemispheric power from *in situ* particle observations

The NOAA/TIROS satellites are in a nearly polar orbit at about 870 km altitude. This orbit takes them across the auroral oval in each hemisphere every 100 minutes. The Total Energy Detector instrument on NOAA/TIROS provide measurements of the directional energy fluxes separately for electrons and ions over the energy range 0.3 to 20 keV and at two pitch angles within the atmospheric loss cone. The observations are processed to obtain a measure of the total energy flux carried into the atmosphere by both electrons and ions along the satellite track. The particle energy flux observations along the satellite track and above 45° magnetic latitude are used to estimate the total amount of power being deposited into the atmosphere in a single, northern or southern, polar region [*Evans* 1987] (see also the web-site at URL: `http://www.sel.noaa.gov`). The method for making this estimate attempts to correct for the way the satellite would traverse a global, statistical pattern of auroral energy deposition taking appropriate account of the spatial expansion and intensification of the pattern of auroral energy deposition with increasing activity. This method requires accumulating observations throughout an entire satellite transit over the polar regions, which requires about 25 minutes, and so is not capable of responding to temporal changes in aurora activity on shorter time scales. The hemispheric power estimates made in this way can also be compromised whenever the spatial pattern of auroral energy deposition departs significantly from the statistical pattern. In spite of these shortcomings, this method of deriving a hemispheric power estimate works remarkably well. The almost continuous coverage since 1978 by successive NOAA/TIROS satellites is particularly useful for long term and statistical studies.

4. The May 19/20, 1996, auroral activity

We selected the period from 17:30 UT, May 19, to 02:30 UT, May 20, 1996, for a detailed comparison. The two hour period before 17:30 UT shows a very quiet auroral oval in the northern hemisphere. The UVI images show a barely visible aurora. At 17:35 UT a small brightening occurs close to magnetic midnight, spreading slowly along the oval towards dusk as well as towards dawn. The aurora brightens and fades occasionally with a slightly increasing brightness until 20:20 UT. At that time a major brightening occurs simultaneously with a significant widening of the auroral oval in the midnight and evening sectors. This auroral activity lasts until about 21:15 UT. Figure 2 shows a few sample images at regular intervals to demonstrate the temporal evolution of the aurora during this period. After the substorm subsides, the aurora remains active showing a structured auroral oval in the evening to midnight sector. A second, larger substorm starts at 00:30 UT on May 20, again leaving a structured oval on the night side. The viewing geometry towards the end of this period becomes less favorable, since the POLAR satellite moves to lower latitudes, such that the auroral zone vanishes partly behind the satellite horizon. As long as the entire auroral oval is in the field of view of the imager, we interpret the total power obtained from integrating over the image as the total hemispheric power. Figure 3 shows the time history of the hemispheric power that we derive from the images. The filter sequence used for this day gave us two LBH-long images every 5 minutes which is therefore the time resolution of the hemispheric power. We also show in the same plot the hemispheric power estimate derived from the *in situ* measurements of two satellites. The NOAA/TIROS 12 and 14 satellite

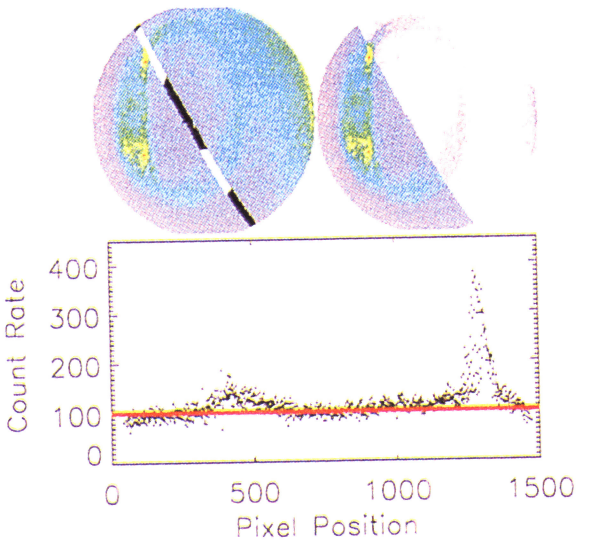

Figure 1. UVI image using the LBH-long filter at 20:30 UT, May 19, 1996. The top left shows the original image with a strip of pixels with common solar zenith angle (70° to 72°) marked. The white section of the strip marks the range from 62° to 77° magnetic latitude. The bottom shows the count rate of all pixels along this strip and (red) the average solar contribution to the total count rates. The count rates are plotted as a function of pixel position, starting at the lower right end of the marked strip. The top right shows the partially processed image after the solar contribution is removed for pixels with solar zenith angle less than 70°.

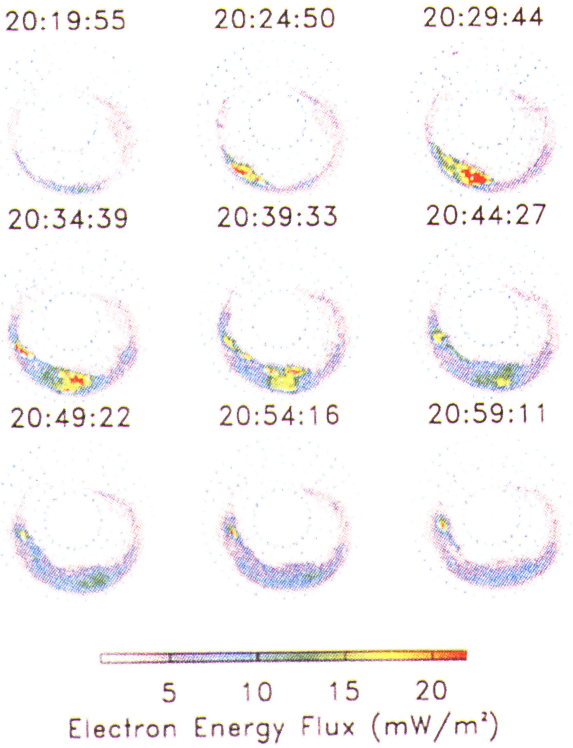

Figure 2. A sequence of 9 energy flux maps in geomagnetic coordinates derived from UVI images. Shown are images at 5 minute intervals from the period 20:20 UT to 20:59 UT. The geomagnetic latitudes of 60°, 70°, and 80° are shown by circles.

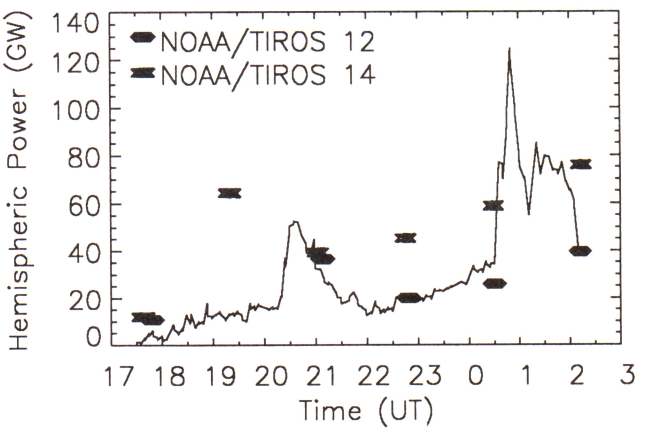

Figure 3. The total hemispheric energy flux from the UVI images as a function of time. The thick horizontal bars show the hemispheric power from the NOAA/TIROS 12 and 14 satellites.

data are shown as thick horizontal bars, which indicate the time over which the data are averaged. The estimated power is normally obtained every 100 minutes for each hemisphere, but is missing for NOAA/TIROS 12 around 19:30 UT because of missing data.

Apparently, NOAA/TIROS 12 only caught the tail end of the first substorm at 20:30 UT, and missed the second substorm at 01:00 UT, as it sampled the northern auroral oval just before and just after the main auroral activity. The NOAA/TIROS 12 satellite was in an orbit passing over the aurora at about 18:30 MLT and 05:30 MLT. The main auroral activity at 00:30 UT started near the midnight sector, which accounts for the NOAA/TIROS 12 missing the active period from 00:30 UT to 02:00 UT. The NOAA/TIROS 14 satellite passed over the auroral oval at the same time, but at a different MLT, from about 14:00 MLT to 04:00 MLT, skimming along the poleward edge of the auroral activity in the morning sector. The UVI images show that NOAA/TIROS 14 sampled the auroral oval in locally enhanced areas at 19:20 UT and 22:45 UT, resulting in an overestimate of the hemispheric power. While NOAA/TIROS 12 missed the beginning of the enhanced activity at 00:30 UT, NOAA/TIROS 14 was closer to the midnight sector where this activity started. This is reflected in the increased power estimate at 00:30 UT. Although the NOAA/TIROS power estimate generally agrees with the power derived from the images, these examples show that the satellite orbit can strongly bias the sampling of auroral activity and lead to erroneous estimates of the hemispheric power. In addition, one can not assume hemispheric symmetry and substitute southern hemisphere satellite data to increase the sampling rate.

5. Summary

Global auroral images in the spectral range of the N_2(LBH) emissions, obtained by the POLAR UVI imager on 19/20 May, 1996, show the entire auroral oval in the sunlit atmosphere. The images were processed to separate the auroral brightness from the dayglow, and the resulting images of the auroral brightness were used to derive the electron energy flux. The total hemispheric power is obtained by spatial integration of the energy flux from the images. Comparison with the hemispheric power estimate derived from NOAA/TIROS energetic particle data shows that sampling along a linear track of once every 100 minutes per hemisphere in a fixed orbital plane leads to satisfactory agreement at times. The NOAA/TIROS data can, however, miss entire substorms or under- or overestimate the hemispheric power due to the limited sampling.

Acknowledgments. This research was supported at the University of Alaska by NASA grant NAG5-1097. We thank NOAA's National Environmental Satellite Data and Information Service for their continued support of the NOAA-TIROS Polar Orbiting Environmental Satellite Program.

References

Craven, J. D., A. C. Nicholas, L. A. Frank, D. J. Strickland, and T. J. Immel, Variations in the FUV dayglow after intense auroral activity, *Geophys. Res. Lett.*, *21*, 2793, 1994.

Evans, D. S., Global Statistical Patterns of Auroral Phenomena, in *Proceedings of the Symposium on Quantitative Modeling of Magnetospheric-Ionospheric Coupling Processes*, 325, Kyoto, 1987.

Fuller-Rowell, T. J., and D. S. Evans, Height integrated Pedersen and Hall conductivity patterns found from the NOAA/TIROS satellite data, J. Geophys. Res., , *92*, 7606, 1987.

Fuller-Rowell, T. J., M. V. Codrescu, R. J. Moffett, and S. Quegan, Response of the thermosphere and ionosphere to geomagnetic storms, J. Geophys. Res., , *99*, 3893, 1994.

Immel, T. J., J. D. Craven, and L. A. Frank, Influence of IMF B_y on large-scale decreases of O column density at middle latitudes, *J. Atm. Terr. Phys.*, *in press*, 1996.

Lu, G., A. D. Richmond, B. A. Emery, and R. G. Roble, Magnetosphere-ionosphere-thermosphere coupling: effect of neutral winds on energy transfer and field aligned current, J. Geophys. Res., , *100*, 19,643, 1995.

Lummerzheim, D. and J. Lilensten, Electron Transport and Energy Degradation in the Ionosphere: Evaluation of the Numerical Solution, Comparison with Laboratory Experiments and Auroral Observations, *Ann. Geophys.*, *12*, 1039, 1994.

Rees, M. H., D. Lummerzheim, and R. G. Roble, Modeling of the Atmosphere-Magnetosphere-Ionosphere System MAMI, *Space Sci. Rev.*, *71*, 691, 1995.

Roble, R. G., E. C. Ridley, A. D. Richmond, and R. E. Dickinson, A coupled thermosphere/ionosphere general circulation model, *Geophys. Res. Lett.*, *15*, 1325, 1988.

Strickland, D., J., J. R. Jasperse, and J. A. Whalen, Dependence of auroral FUV emissions on the incident electron spectrum and neutral atmosphere, *J. Geophys. Res.*, *88*, 8051, 1983.

Torr, M. R., D. G. Torr, M. Zukic, R. B. Johnson, J. Ajello, P. Banks, K. Clark, K. Cole, C. Keffer, G. Parks, B. Tsurutani, J. Spann, A far ultraviolet imager for the international solar-terrestrial physics mission, *Space Sci. Rev.*, *71*, 329, 1995.

D. Lummerzheim, University of Alaska, Geophysical Institute, Fairbanks, AK 99775-7320. (E-mail: lumm@loke.gi.alaska.edu)

M. Brittnacher, G. K. Parks, University of Washington, Geophysics Program, Seattle, WA 98195-1650

D. Evans NOAA, Space Environment Center, Boulder, CO 80303

G. A. Germany, University of Alabama, Huntsville, AL 35899

M. H. Rees, Physics Department, University of Southampton, Southampton, SO17 1BJ England

J. F. Spann Marshall Space Flight Center, Huntsville, AL 35812

(Received September 27, 1996; accepted November 27, 1996.)